NIH Public Access
Author Manuscript
Biochemistry. Author manuscript; available in PMC 2011 August 24.

Published in final edited form as:
Biochemistry. 2010 August 24; 49(33): 7108–7118. doi:10.1021/bi1006095.

Chaperone-like *N*-methyl Peptide Inhibitors of Polyglutamine Aggregation†

Jennifer D. Lanning[‡], **Andrew J. Hawk**[‡], **JohnMark Derryberry**[‡], and **Stephen C. Meredith**[‡,§,*]

[(‡)]Department of Pathology, The University of Chicago, Chicago, IL 60637, USA

[(§)]Department of Biochemistry and Molecular Biology, The University of Chicago, Chicago, IL 60637, USA

Abstract

Polyglutamine expansion in the exon 1 domain of huntingtin leads to aggregation into β-sheet-rich insoluble aggregates associated with Huntington's Disease. We assessed eight polyglutamine peptides with different permutations of *N*-methylation of backbone and side chain amides as potential inhibitors of polyglutamine aggregation. Surprisingly, the most effective inhibitor, $5QMe_2$ (Anth-K-Q-Q(Me2)-Q-Q(Me_2)-Q-$CONH_2$, Anth = *N*-methyl anthranilic acid, Q(Me_2) = side chain *N*-methyl Q) has only side chain methylations at alternate residues, highlighting the importance of side chain interactions in polyglutamine fibrillogenesis. Above a 1:1 stoichiometric ratio, $5QMe_2$ can completely prevent fibrillation of a synthetic aggregating peptide $YAQ_{12}A$; it also shows significant inhibition at substoichiometric ratios. Surface plasmon resonance (SPR) measurements show a moderate K_d with very fast k_{on} and k_{off}. Sedimentation equilibrium analytical ultracentrifugation indicates that $5QMe_2$ is predominantly or entirely monomeric at concentrations up to 1 mM, and that it forms a 1:1 stoichiometric complex with a fibril-forming target, $YAQ_{12}A$. $5QMe_2$ inhibits not only nucleation of $YAQ_{12}A$, but also fibril extension, as shown by the fact that it also inhibits seeded fibril growth where the nucleation steps are bypassed. $5QMe_2$ acts on its targets only when they are in the PPII-like conformation, but not after they undergo a transition to β-sheets. Thus $5QMe_2$ does not disassemble pre-formed $YAQ_{12}A$; this contrasts with our previously described, backbone *N*-methylated inhibitors of β-amyloid aggregation (16,17). The mode of action of $5QMe_2$ is reminiscent of chaperones, since it binds and releases its targets very rapidly, and maintains them in a non-aggregation-prone, monomeric state, in this case, the polyproline II (PPII)-like conformation, as shown by CD spectroscopy.

Expanded polyglutamine (polyQ) tracts are responsible for at least nine neurodegenerative diseases, including Huntington's Disease (HD). HD occurs when the polyQ domain of exon

†We acknowledge NIH Medical Scientist Training Program Grant (T32 GM07281 JDL), NIH Cardiovascular Pathophysiology Training Grant (HL07237 JDL) and NIH (NS042852 SCM) and the Alzheimer's Association (IIRG-06-27794).

*To whom correspondence should be addressed: Department of Pathology, 5841 S. Maryland Ave., Chicago, IL 60637. Tel: 773-702-1267. Fax: 773-834-5251. scmeredi@uchicago.edu .

Supporting Information Available The following items are available as supporting information: A derivation of the equations and other details needed for analysis of equilibrium sedimentation analytical ultracentrifugation of two dissimilar interacting species; determination of $\bar{v}$, for $YAQ_{12}A$ and $5QMe_2$; reverse phase HPLC isocratic analysis of $YAQ_{12}A$ remaining in solution, in the presence or absence of $5QMe_2$; experiments showing the effect of added fibril seeds on fibrillation of $YAQ_{12}A$; electron micrograph of fibril seed slurry used in preceding experiments; example of analytical ultracentrifugation of $YAQ_{12}A$ and $5QMe_2$, showing no improvement of fit from the addition of higher order terms in either species; table of comparison of data fits, according to the Aikake Information Criterion, showing improvement of fits by adding a term for a complex between $YAQ_{12}A$ and $5QMe_2$; calibration of Superdex Peptide 10/300 GL column with molecular weight standards; and data showing the absence of a small zone effect in chromatography using the Superdex Peptide column. This material is available free of charge at http://pubs.acs.org.

NIH-PA Author Manuscript
NIH-PA Author Manuscript
NIH-PA Author Manuscript

NIH-PA Author Manuscript

NIH-PA Author Manuscript

NIH-PA Author Manuscript

1 of huntingtin protein expands beyond a threshold of approximately 35 residues (1), leading to polyQ aggregation (2-4). PolyQ proteins can form β-sheet rich fibrils (5,6). In contrast to many other amyloids (7), polyQ domains have polar side chains, and both these and backbone atoms can form hydrogen bonds. Recent x-ray diffraction and solid-state NMR studies of the glutamine- and asparagine-rich yeast prion proteins Sup35p and Rnq1p show parallel in-register β-sheet segments, possibly separated by non-β-sheet bend structures in longer peptides (8,9). Prefibrillar oligomers of β-amyloid are micelle-like and show β-sheet character (10). The structure of polyQ oligomers is not known, however; in contrast to oligomers of β-amyloid, the polar nature of poly Q makes it unlikely that they would be micelle-like. Large, prefibrillar “spheroids” of huntingtin also have been observed, and these acquire β-sheet structure as they mature into fibrils (11). We have recently shown that small, soluble oligomers of short polyQ peptides adopt a polyproline-II helix-like structure (12,18), and thus the conversion to fibrils may require a transition from this structure to β-sheet.

Inhibitors of protein and peptide aggregation are of value both as molecular probes of the aggregation pathway and as potential therapeutic agents (13-15). We have described peptidic inhibitors of β-amyloid, consisting of an aggregation domain in which alternate residues are *N*-methylated on backbone amides. Such inhibitors (e.g., Aβ16-20m) both inhibit fibril formation and disassemble preformed fibrils, by disrupting backbone hydrogen bonding (16,17).

In this paper, we describe what began as a comparison of *N*-methylation patterns in potential inhibitors of polyQ peptide aggregation. These studies, however, soon produced several surprising results, starting with the observation that side chain *N*-methylations alone yield the most effective inhibitors of all the permutations tested on short polyQ peptides. Subsequent experiments highlighted the importance of side chain interactions in polyQ aggregation, and showed that the inhibitors act through a mechanism reminiscent of chaperone proteins. We examined the most effective of these inhibitors in detail, and observed that it binds to a target polyQ peptide and inhibits its aggregation by forming a 1:1 stoichiometric complex. It inhibits not only nucleation, but also fibril extension, as shown by its ability to inhibit seeded fibril growth in which nucleation steps are bypassed. Furthermore, our data indicate that the effective inhibitors adopt a polyproline II conformation, and interact with a polyQ peptide only while it is also in the PPII conformation. These results suggest a more complex scheme for the polyglutamine aggregation pathway than has been appreciated previously.

Experimental Procedures

Peptide Synthesis and Purification

$YAQ_{12}A$ and 5Q were synthesized using standard 9-fluorenylmethoxycarbonyl (FMOC) chemistry and Rink Amide resin, on an Applied Biosystems Model 431A peptide synthesizer. In early experiments, peptides were cleaved from the resin using 9.5 mL of TFA, 0.25 mL of water and 0.25 mL of triisopropylsilane. We subsequently observed that both yields and initial purity of the mixture from the resin were significantly improved by cleaving peptide from the resin using a mixture or 9 mL TFA, 0.5 mL thioanisole, 0.3 mL ethanediol, and 0.2 mL anisole for 1 h.

Peptides with backbone *N*-methyl groups were synthesized manually according to Biron *et al*. (19). Peptides with side chain methylations were synthesized on tBoc 4-Methylbenzhydrylamine (MBHA) resin at 0.25 mmol scale, either manually for peptides containing backbone *N*-methyl groups, or using the synthesizer for peptides with no backbone *N*-methyl groups. Side chain *N*-methyl Gln residues were prepared by deprotecting Glu(tBu) side chains on resin (TFA:H_2O, 95:5, v:v), and then amidating (22°C,

NIH-PA Author Manuscript

NIH-PA Author Manuscript

NIH-PA Author Manuscript

overnight) under N_2 with 1 mmol benzotriazole-1-yl-oxy-tris-(dimethylamino)-phosphonium hexafluorophosphate (BOP), 2 mL 2.0 M dimethylamine in methanol, 5 mL dimethylformamide (DMF); this procedure was repeated for an additional 4 h. Although BOP is a less efficient coupling agent than HATU (2-(7-Aza-1H-benzotriazole-1-yl)-1,1,3,3-tetramethyluronium hexafluorophosphate), the latter reagent gave guanylation side products during long incubations. In one peptide, 5MeQ-PEG-5MeQ (see Figure 1A), a PEG moiety, FMOC-8-amino-3,6-dioxaoctanoic acid ("FMOC-mini-PEG", Peptides International) was incorporated into the middle of the peptide. After incorporation of the PEG group, the remaining amino acids were incorporated into the peptide as described above.

The MBHA resin was washed with DMF, and peptide was cleaved and deprotected using anhydrous HF:*p*-cresol (10:1, v:v, 0°C). After the peptides were precipitated in ice-cold diethyl ether, they were purified using by C18 preparative HPLC (Zorbax) at 22 °C, either with a water:acetonitrile (both 0.1% TFA, v:v) gradient, or with an isocratic mixture. Peptide purity was ≥ 95% by analytical HPLC. Molecular masses of the peptides were verified with ESI- and MALDI-TOF mass spectrometry. A Lys residue was incorporated into all inhibitor peptides to aid cellular ingress of peptides (for studies not included herein) and possibly to increase solubility. N-terminal *N*-methyl anthranilic acid was added to allow detection by fluorescence and UV spectroscopy.

Dissolving and Disaggregation of $YAQ_{12}A$; Sedimentation Assays of $YAQ_{12}A$ Aggregation

Aggregation of $YAQ_{12}A$ was measured as the concentration of monomeric peptide remaining in solution after sedimentation, as described elsewhere (20). The elution of 100 μM $YAQ_{12}A$ in Size Exclusion Chromatography was most consistent with monomeric state. Chromatography was performed using a Superdex Peptide 10/300 GL column (GE Lifesciences) equilibrated with 10 mM sodium phosphate, pH 7.40; the flow rate was 0.5 mL/min (see Figure 2F and G). Apparent molecular weight (MW^{app}) was estimated on the basis of a calibration curve of molecular weight standards (Supporting Figure 4). Additional size exclusion chromatography experiments are described below.

Concentration was determined by absorbance at 274.6 nm, using an extinction coefficient (ε) of 1420 $M^{-1}cm^{-1}$. The solution was diluted to 100 μM with 10 mM sodium phosphate, pH 7.40, and incubated with or without inhibitor peptides for various times at 37 °C without agitation. After incubation, the mixture was centrifuged in an Airfuge ultracentrifuge (Beckman) at 98,000 × g for 1 h at 22 °C. 100 μL of the top third of the resulting solution was injected onto an analytical C18 RP-HPLC column and followed by absorbance at 220 nm. The concentration of $YAQ_{12}A$ injected was calculated from the peak area data compared to a standard curve made from solutions of $YAQ_{12}A$ of known concentrations. In more recent experiments, we were able to shorten the time between analyses by performing isocratic analyses; using a Zorbax C18 column, and an eluent of water:acetonitrile:TFA (87.5:12.5:0.1, v:v:v), $YAQ_{12}A$ elutes at ~ 6 minutes and $5QMe_2$ elutes at ~ 22 minutes (Supporting Figure 1).

Stock solutions of inhibitor peptides at ~ 4 mM were made from pure lyophilized peptide and MilliQ purified water, adjusted to 7.00, since pH affects ε of *N*-methyl anthranilic acid. Concentration of the stock was determined by absorbance using $\varepsilon_{337\ nm} = 2690\ M^{-1}cm^{-1}$. Aliquots at various concentrations were frozen, lyophilized, and stored at −20 °C. All fibrillation reactions were performed in siliconized microfuge tubes.

NIH-PA Author Manuscript

NIH-PA Author Manuscript

NIH-PA Author Manuscript

Additional Size Exclusion Chromatography Experiments

As stated above, initial experiments showed that $YAQ_{12}A$, disaggregated as described above, eluted from a Superdex Peptide column in a position most consistent with a monomeric state. To examine the time course of this chromatographic behavior, and the effect of the aggregation inhibitor peptide $5QMe_2$ described in Results, we performed the following series of size exclusion chromatography experiments. A 100 μM solution of freshly disaggregated $YAQ_{12}A$ was chromatographed either alone or in the presence of 170 μM $5QMe_2$. (In other experiments, a 1:1 molar ratio of $YAQ_{12}A$:$5QMe_2$ was used; see, for example, Supporting Figure 5). To make the mixture of peptides, $5QMe_2$ was dissolved in water:TFA (100:0.1, v:v) and distributed into siliconized microfuge tubes. Solvent was evaporated under a stream of N_2 followed by lyophilization. To the dry film, $YAQ_{12}A$ solutions were added. After 0, 24 and 50 h of incubation of these solutions are 37 °C, a 100 μL aliquot of each solution was injected onto a Superdex Peptide 10/300 GL column. Mobile phase was 10 mM sodium phosphate containing 10 mM NaCl, pH 7.40. Flow rate was 0.5 ml/min. The column effluent was monitored at 220, 230, 274 and 337 nm. Essentially the same chromatographic pattern was observed at each wavelength, except that only $5QMe_2$ could be observed at 337 nm, where the *N*-methyl anthranlate moiety absorbs.

Inhibition of Seeded $YAQ_{12}A$ Fibril Growth by $5QMe_2$

To produce fibril seeds, $YAQ_{12}A$ fibrils were made by incubating a 250 μM solution of the peptide, initially dissolved as described above, at 37 °C for at least one week. Immediately prior to the seeding experiment, the seed slurry was sonicated for five minutes using a Bransonic ultrasonic bath (Model: 2510R-MT, Branson Ultrasonics Corp., CT). In preliminary experiments, we assessed the effects of adding various nominal concentrations of $YAQ_{12}A$ fibril seeds to a fresh, 100 μM solution of $YAQ_{12}A$ (see Supporting Figure 2A; Supporting Figure 2B shows that the seeds were indeed fibrillar). Nominal concentration of the seed slurry was defined from the original peptide concentration of the solution from which the seed slurry was made. From these experiments, we determined that a nominal concentration of 8 μM was optimal for this batch of seed fibrils in order to observe both accelerated fibrillation of fresh $YAQ_{12}A$, and the effects of $5QMe_2$ on seeded fibril growth.

For the seeding experiments, we compared $YAQ_{12}A$ fibrillation in the presence or absence of fibril seeds, and in the presence or absence of $5QMe_2$. $YAQ_{12}A$ was freshly disaggregated, and dissolved in 10 mM phosphate (with 1 μM NaN_3), to a concentration of approximately 150 μM. Actual concentration was determined by absorbance at 274.6 nm, and confirmed by injecting an aliquot onto an analytical C18 RP-HPLC column, as described above. Siliconized microfuge tubes were prepared with or without a sufficient of $5QMe_2$ so that the final concentration of this peptide would be 100 μM. To this mixture, sufficient buffer was added so that the to final volume would be 600 μL and the final $YAQ_{12}A$ concentration would be 100 μM. Lastly, an aliquot of the above fibril seed slurry was added to some samples to give a final nominal seed concentration of 8 μM. Thus, in those samples containing $5QMe_2$, the molar ratio of $YAQ_{12}A$:$5QMe_2$ was 1:1. The mixtures were incubated at 37 °C for 0 h, 5 h, 24 h or 50 h. At each time point, fibrillation was assessed by the above sedimentation assay, performed at least in triplicate; results are reported as mean ± S.D.

Electron Microscopy

Electron microscopy was performed as described elsewhere (16); micrographs were recorded at magnifications of 15,000 or 39,000×, plus 1.4× magnification from the CCD camera.

NIH-PA Author Manuscript

NIH-PA Author Manuscript

NIH-PA Author Manuscript

Surface Plasmon Resonance

$YAQ_{12}A$ that had been disaggregated and centrifuged as described (20), was immobilized on a CM5 sensor chip using standard amine coupling procedures, as described by the manufacturer's instructions (Pharmacia Biosensor AB). All assays were carried out using a Biacore 3000 instrument at 25 °C, at a flow rate of 20 μL/min, with association and dissociation times of 120 s, in HSP-B buffer (Biacore). Each concentration of analyte was tested in triplicate. Kinetics data were analyzed first using BIA evaluation software (Biacore), and then by non-linear least squares analysis using Kaleidagraph software and using a non-linear least squares fitting program described by Yamaoka et al. (21). Adsorption kinetics were fitted as a bimolecular interaction of the analyte ($5QMe_2$) interacting with the immobilized ligand ($YAQ_{12}A$), forming the 1:1 complex at the sensor surface. The best fit (see below, Figure 3), was obtained with single exponential equations for association and dissociation. Specifically, during association, the SPR signal varied with time as given by the equation:

$$R_t = \frac{k_{on}[I]B_{max}}{k_{on}[I] + k_{off}} \times \left(1 - e^{-(k_{on}[I] + k_{off})t}\right) \quad \text{[Eq. 1]}$$

where R_t is the SPR signal ("response units" or RUs) as a function of time, kon and k_{off} are association and dissociation constants, respectively, B_{max} is maximum binding capacity, and t is time in seconds. Similarly, during dissociation the SPR signal varied according to the equation:

$$R_t = R_{eq}\left(e^{-k_{off}\,t}\right) \quad \text{[Eq. 2]}$$

where R_{eq} is the signal reached at equilibrium. Both equations, for association and dissociation are as described by DeMol and Fischer (22). Figure 3, shown in Results, represents a global fit of all data using single values for k_{on} and k_{off}. Dissociation constant, K_d, was calculated as k_{off}/k_{on}.

Circular Dichroism

Circular dichroic (CD) spectra were recorded using an AVIV 202 spectropolarimeter. Lyophilized inhibitor peptides were dissolved directly in 10 mM phosphate buffer, pH 7.40. Monomeric 50 μM $YAQ_{12}A$ was prepared as described above in the same buffer. Spectra were obtained at 22 °C, with a 1 mm cuvette; five scans were averaged and contributions from buffer were subtracted; data were smoothed using a macro in Kaleidagraph software.

Fibril film CD spectra were measured essentially as described by Darnell et al. (12). Briefly, a concentrated slurry of fibrils was obtained by first centrifuging the slurry in a microfuge for 5 minutes, and resuspending the pellet in the same buffer; 20 μl aliquots of the slurry in five μl droplets were placed onto cut quartz plates (12.5 mm × 12.5 mm, Starna) and allowed to coalescence into one aqueous film. All samples were dried under vacuum overnight at room temperature. Spectra were taken immediately after removing the plates from vacuum, using an Aviv model 202 spectropolarimeter (Lakewood, NJ) at one nm intervals from 260 nm to 190 nm with a one sec averaging time, a one nm bandwidth, and at 25 °C. To determine whether linear dichroism was present, spectra were again recorded after the plates were rotated by 90°. Any samples that exhibited shifts in maxima or minima were discarded from the data set. Data sets showing scatter after 90° rotation were still used. Spectra shown in Results represent the averages of five scans for each film. Spectra are presented as wavelength versus background corrected raw ellipticity signal.

NIH-PA Author Manuscript

NIH-PA Author Manuscript

NIH-PA Author Manuscript

Analytical Ultracentrifugation: Experimental Procedure

Equilibrium sedimentation analytical ultracentrifugation was performed using a Beckman Optima XLA ultracentrifuge equipped with an An-60Ti rotor with six-sector cells. Solutions of monomeric 100 μM $YAQ_{12}A$ were prepared as described above in 10 mM sodium phosphate, pH 7.40. This peptide sample was added to lyophilized aliquots of $5QMe_2$, yielding final inhibitor concentrations of 100 μM (molar ratio 1:1, $YAQ_{12}A$:$5QMe_2$), 500 μM (molar ratio 1:5, $YAQ_{12}A$:$5QMe_2$) and 1 mM (molar ratio 1:10, $YAQ_{12}A$:$5QMe_2$). Of the four cells in the rotor, one contained buffer only (10 mM sodium phosphate, pH 7.40), two were duplicates, each containing the three above described mixtures of $YAQ_{12}A$ and $5QMe_2$, while the last contained samples of $5QMe_2$ alone at 100 μM, 500 μM, and 1mM. Sedimentation was monitored at 230 and 280 nm, at 20 °C, with an hour between scans. Rotor speed progressed from 3000 rpm (1 scan) to 36,000 rpm (16 scans) to 48,000 rpm (13 scans) to 60,000 rpm (19 scans). Equilibrium was demonstrated by the absence of change in absorbance profile over the course of at least 8 hours.

Sedimentation equilibrium analytical ultracentrifugation data were analyzed using an approach that derives in part from previous methods for analyzing the formation of complexes by two dissimilar species, interacting at sedimentation equilibrium in an ultracentrifugal field (23-26). Absorbances used for analysis were at 280 nm, except $5QMe_2$ alone at 100 μM, which was followed at 230 nm for greater sensitivity at the lower concentration. Additional details of analysis, including derivation of equations, and methods for determination of $\bar{v}$ (27), are given in Supporting Information.

Results

Sedimentation Screening Assays

To screen peptides as potential polyQ fibrillation inhibitors, we used $YAQ_{12}A$, a synthetic polyQ peptide that forms fibrils over the course of several days, making it amenable to kinetic analysis. In addition, in contrast to longer polyQ peptides, $YAQ_{12}A$ can be highly purified. Thus, our assay consisted of measuring fibrillation in the presence and absence of potential inhibitor peptides. The potential inhibitors tested are shown in Figure 1A. Fibrils of short polyQ peptides such as $YAQ_{12}A$ cause very little or no appreciable thioflavin T fluorescence, however. For this reason, we used sedimentation assays (20) to follow the aggregation of $YAQ_{12}A$ in the presence and absence of inhibitor peptides. For the purpose of performing screening assays, high inhibitor concentrations were used (4 mM inhibitor:0.1 mM $YAQ_{12}A$). In the absence of inhibitors, after incubating 100 μM $YAQ_{12}A$ for 40 hr at 37 °C, 8.8 ± 0.3 μM (mean ± S.D.) monomer remained in solution (Figure 1B).

The first inhibitor tested was $5MeQMe_2$, which contained both backbone and side chain glutamine *N*-methylations to disrupt hydrogen bonds at both locations. Alternate residues were modified to leave some amides available for binding to $YAQ_{12}A$ (16,17). This peptide and subsequent ones discussed in this paper also contain additional moieties, as in our earlier studies on inhibitors of β-amyloid and human prion peptide ($PrP_{106-126}$) aggregation (16,17). N-Me-anthranilic acid was added for fluorescence detection in cellular studies (not discussed herein); the single Lys residue and C-terminal carboxamidation are also used to favor ingress of the peptides into cells (17) and the Lys residue may also increase solubility.

Although incubation of $5MeQMe_2$ with $YAQ_{12}A$ did show significant inhibition (36.8 ± 3.7 μM monomeric $YAQ_{12}A$ remaining in solution, Figure 1B), this inhibitor was considerably less effective than expected, given that it was present a 40:1 molar concentration relative to $YAQ_{12}A$.

NIH-PA Author Manuscript

NIH-PA Author Manuscript

NIH-PA Author Manuscript

We then attempted to optimize the inhibitor. Lengthening the core glutamine sequence from 5 residues to 7 ($7MeQMe_2$) resulted in a *less* effective inhibitor, (24.7 ± 1.7 μM). Based on the hypothesis that methylating *both* side chain and backbone amides might hinder binding of inhibitor to $YAQ_{12}A$, we synthesized 5MeQ, which has only backbone *N*-methylations. 5MeQ proved to be slightly more effective than the other inhibitors (42.2 ± 1.7 μM). We also attempted to model a proposed polyQ fibril structure (8,9) by connecting two 5MeQ peptides either with a tight β-hairpin turn (^{D}Pro-Gly sequence) or a flexible linker (PEG, polyethylene glycol). These peptides were moderately effective as inhibitors, yielding 31.6 ± 1.0 and 51.5 ± 4.0 μM monomeric $YAQ_{12}A$ remaining in solution, respectively.

Surprisingly, $5QMe_2$, with only side chain methyl groups (again, on alternate residues), completely inhibited aggregation of $YAQ_{12}A$, with essentially all of the $YAQ_{12}A$ remaining in solution at the end of the incubation (91 ± 0.6 μM). $(QMe_2)_5$, with side chain methylations on all Q residues, was *less* effective (58.9 ± 0.9 μM monomeric $YAQ_{12}A$ remaining) than $5QMe_2$, demonstrating the importance of the alternating pattern of methylated residues. Finally, the unmethylated peptide, 5Q, was not inhibitory; after incubating 5Q with $YAQ_{12}A$, the concentration of the latter peptide remaining in solution was 11.9 ± 1.7 μM, similar to $YAQ_{12}A$ alone.

Time Course of Inhibition of $YAQ_{12}A$ Aggregation by $5QMe_2$ and Electron Microscopy of Reaction Products

We then focused on $5QMe_2$, by far the most effective of these inhibitors. Size exclusion chromatography confirmed that the top ultracentrifugal fraction of disaggregated $YAQ_{12}A$ used for these assays was most consistent with monomeric molecular weight (Figure 2F and 2G; see also Supporting Figure 4A and B). Sedimentation assays showed that $YAQ_{12}A$ monomer shows a monoexponential decline over 110 h, without a lag period ($k = 0.04\ h^{-1}$, Figure 2A). When 100 μM $YAQ_{12}A$ was incubated with 100 μM $5QMe_2$, we observed a lag period, in which soluble $YAQ_{12}A$ declined slowly, followed by more rapid loss of this peptide from solution after ~ 70 h. When 100 μM $YAQ_{12}A$ was incubated with 1 mM $5QMe_2$, no aggregation was observed for the entire time period. Electron microscopy confirmed the sedimentation assay results. Incubation of $YAQ_{12}A$ with $5QMe_2$ (500 μM, for Figure 2E) abrogates fibril formation at 40 h.

As stated, in the absence of inhibitor, much of the $YAQ_{12}A$ initially in solution precipitated and formed fibrils. As shown in Figure 2F and 2G, however, at 0, 24 and 50 h, essentially all of the $YAQ_{12}A$ in solution eluted from the size exclusion chromatography column at a position most consistent with monomeric molecular weight. If any oligomeric $YAQ_{12}A$ was in solution at these three times, it represents a very small and probably kinetically transient fraction of the total $YAQ_{12}A$ in solution. The effect of adding $5QMe_2$ to $YAQ_{12}A$ was to keep the latter peptide in solution for a longer period of time, but $5QMe_2$ did not alter the chromatographic behavior of $YAQ_{12}A$. As shown in Figure 2G, at increasing times, more $YAQ_{12}A$ remained in solution in the presence than in the absence of $5QMe_2$. The chromatographs show two well-resolved peaks, one each in the positions previously observed for $YAQ_{12}A$ and $5QMe_2$. In the presence of $5QMe_2$, essentially all of the $YAQ_{12}A$ was still in solution at 24 h, as shown by the fact that the size of the peak was essentially unchanged from that at 0 h of incubation. At 50 h, the $YAQ_{12}A$ peak was slightly smaller than that seen at 0 or 24 h, but no additional peaks were observed. We demonstrate below that these two peptides form a complex, with K_d ~ 1 μM. The absence of a peak for this complex is consistent with dissociation of a complex of this affinity during chromatography.

NIH-PA Author Manuscript

NIH-PA Author Manuscript

NIH-PA Author Manuscript

Effect of Adding Inhibitor at Various Points in the Time Course of Aggregation

Many aggregating peptides are believed to form fibrils by a rate limiting nucleation step followed by elongation of the nucleus (3,5,28,29). To learn whether $5QMe_2$ could prevent aggregation of $YAQ_{12}A$ when added at different stages during 70 h of fibril formation, we added 1 mM $5QMe_2$ to 100 μM $YAQ_{12}A$ 10 or 20 h after the start of incubation (Figure 2B). Monomeric $YAQ_{12}A$ remaining after 70 h was then assessed by sedimentation assay. $5QMe_2$ was able to prevent all but a modest further decline in monomer concentrations, regardless of the time of addition. These experiments suggest that $5QMe_2$ may act to disrupt both nucleation and elongation steps and maintain $YAQ_{12}A$ in its monomeric state. The inhibitor did not reverse aggregation, however, as no additional monomer appeared in solution after incubation of the mixture with the inhibitor.

Inhibition of Seeded $YAQ_{12}A$ Fibril Growth by $5QMe_2$

These experiments were designed to assess the whether $5QMe_2$ could inhibit precipitation of $YAQ_{12}A$ from solution in the presence of pre-formed fibril seeds. The results shown in Figure 2A and 2E indicate that $5QMe_2$, when added to $YAQ_{12}A$ at the start of a fibrillation reaction, can act as a nucleation inhibitor. That is, $5QMe_2$ can prevent or delay growth of fibrils under unseeded fibrillation conditions. The data shown in Figure 2B suggest that $5QMe_2$ can also act as a fibril extension inhibitor, since addition of $5QMe_2$ 10 or 20 h after the start of the reaction prevented nearly all additional precipitation of $YAQ_{12}A$ from solution. To test further the idea that $5QMe_2$ can act as a fibril extension inhibitor, we examined seeded growth of $YAQ_{12}A$. In particular, pre-formed fibril seeds were added to disaggregated solutions of $YAQ_{12}A$, with or without $5QMe_2$, as described in Methods. As a control experiment, the same incubations were performed without the addition of $YAQ_{12}A$ seeds. The results of these experiments are shown in Figure 3. The data in Figure 3A for unseeded fibril growth is similar to that shown in Figure 2: in unseeded, freshly disaggregated solutions of $YAQ_{12}A$, peptide spontaneously precipitates and forms fibrils, and the addition of $5QMe_2$ inhibits fibrillation, causing the $YAQ_{12}A$ to remain in solution. When $YAQ_{12}A$ fibrils are added to fresh, disaggregated solutions of $YAQ_{12}A$ (Figure 3B), more $YAQ_{12}A$ is lost from solution at each time point than in the absence of added seeds. Thus, the added fibrils do indeed seed fibrillation. When $5QMe_2$ is also added to the mixture of fibril seeds and fresh $YAQ_{12}A$ solutions, it inhibits loss of soluble $YAQ_{12}A$ into the insoluble fraction. Since the addition of fibril seeds largely bypasses nucleation, these data indicate that $5QMe_2$ inhibits fibril extension. Thus, $5QMe_2$ is both a nucleation and fibril extension inhibitor.

Inhibitor Concentration Dependency

We examined the inhibitor concentration dependency using sedimentation assays. 100 μM $YAQ_{12}A$ was incubated 40 h with various concentrations of $5QMe_2$, at molar ratios ranging from 40:1 to 1:10 ($5QMe_2$:$YAQ_{12}A$), and after ultracentrifugation, the top fraction was assayed for soluble $YAQ_{12}A$. As shown in Table 1, inhibition was essentially complete at ratios of 1:1, but was significant even at a substoichiometric ratio of 1:10 ($5QMe_2$:$YAQ_{12}A$).

Kinetics of $YAQ_{12}A$ and $5QMe_2$ Binding, as Assessed by Surface Plasmon Resonance (SPR)

After observing that $5QMe_2$ could inhibit aggregation of $YAQ_{12}A$ at substoichiometric levels, we investigated the affinity and kinetics of $YAQ_{12}A$ and $5QMe_2$ binding with surface plasmon resonance (SPR). We reasoned that $5QMe_2$ could act at substoichiometric ratios by interacting transiently and sequentially with monomeric $YAQ_{12}A$ molecules. SPR experiments showed rapidly reversible binding and dissociation of $5QMe_2$ to immobilized

NIH-PA Author Manuscript

NIH-PA Author Manuscript

NIH-PA Author Manuscript

$YAQ_{12}A$ at a range of inhibitor concentrations. Figure 4A shows a global fit of the data to monoexponential rate equations (described in Methods); Figure 4B shows residuals (differences between experimental values and theoretical fits). From these analyses, k_{on} and k_{off} for each set of triplicate runs were 0.026 μM s^{-1} and 0.024 s^{-1}, respectively, yielding a value of 0.92 μM for K_d. Data for individual curves were also analyzed using the same equations, and the numbers obtained for k_{on}, k_{off}, and K_d (representing an arithmetic mean of the values) were .030 μM s^{-1}, 0.026 s^{-1}, and 0.87 μM, respectively, in reasonable agreement with the numbers obtained from global fitting. These data indicate very rapid association and dissociation of predominantly a 1:1 complex of $YAQ_{12}A$ and $5QMe_2$, and moderate affinity. The rapidity of binding and dissociation is reminiscent of chaperones, which act substoichiometrically by making rapid, transient complexes with sequential molecules of their targets.

AUC and Complex Stoichiometry

We used sedimentation equilibrium analytical ultracentrifugation experiments to analyze the complex (IQ) formed from $YAQ_{12}A$ (Q) and $5QMe_2$ (I). We first demonstrated that the inhibitor alone is monomeric at three concentrations (100, 500, and 1000 μM, and at three rotor speeds (Figure 5). The experimental molecular weight (mean ± S.D. for all of the above conditions) for $5QMe_2$ at these concentrations was 975.2 ± 32.1, very close to the expected value of 976 g/mol. When the results for the three concentrations were analyzed globally, the molecular weights obtained were 988.5, 1000.0, and 980.1 for rotor speeds of 36,000, 48,000 and 60,000 rpm, respectively. This is again in agreement with the expected molecular weight for $5QMe_2$.

The complex formed between I and Q was analyzed using the experimental procedures described by Winzor *et al*. (23), which is based on earlier papers of the same group (24-26). A description of this technique, including derivations of equations as used in the experiments on these particular peptides, is given in detail in the Supporting Information. Briefly, sedimentation equilibrium data are analyzed according to the equation,

$$A_t(r) = C_I(r_F)\,\varepsilon_I\psi_I(r) + C_Q(r_F)\,\varepsilon_Q[\psi_I(r)]^p + C_{IQ}(r_F)\,\varepsilon_{IQ}[\psi_I(r)]^{p+1} + C_{I2Q}(r_F)\,\varepsilon_{I2Q}[\psi_I(r)]^{p+2} + \ldots \quad \text{[Eq. 3]}$$

where $C_i(r)$ is the concentration of each species at each radial position, r, in the ultracentrifugal field. The function $\Psi_i(r)$ is defined as $\exp[M_i\phi_i(r^2 - r_F^2)]$, where $\phi_i = \frac{\left(1 - \bar{v}_i\rho\right)\omega^2}{2RT}$, and M_i is molecular weight of each species, r_F is an arbitrarily chosen fixed radial distance from the center of rotation, $\bar{v}$ is the partial specific volume of each species, ω is angular velocity, ρ is solvent density, T is temperature (K), and R is the gas constant. For synthetic peptides, the values of M_i are known; here, M_I = 976, M_Q = 1860, M_{IQ} = 2736, and so forth for other types of complexes. The parameter, p is defined as $M_i\phi_i/M_j\phi_j$; in the present experiments, i = Q and j = I, and thus p = 1.90.

In these experiments, sedimentation equilibrium ultracentrifugation was performed using three sets of peptide concentrations, either an equimolar concentration of I and Q (100 μM of each), or excess of the inhibitor (500 or 1000 μM of I with 100 μM of Q). In addition, the sample was centrifuged to equilibrium at three angular velocities, 36000, 48000, and 60000 rpm. It was necessary to use equimolar or higher inhibitor concentration because at lower concentrations of the inhibitor, Q would not stay in solution, as is also indicated in Figure 2.

The null hypothesis to be tested in these experiments is that, in agreement with SPR data, the predominant complex between I and Q is a 1:1 complex. Under the conditions used in

NIH-PA Author Manuscript

NIH-PA Author Manuscript

NIH-PA Author Manuscript

these experiments (equimolar or excess I compared to Q) and given the K_d (0.92 μM) obtained from SPR, the expected concentration of Q is low compared to those of either I or IQ, and also with respect to the experimental error in measurement of absorbance. For this reason, the results were analyzed in two, complementary ways, as follows.

First, the data were analyzed according to Eq. 3, and the value of K_d was evaluated from the values of the three parameters, $C_I(r_F)$, $C_Q(r_F)$, and $C_{IQ}(r_F)$. Second, we used the value of K_d obtained from SPR experiments to calculate the least precise (because it has the lowest value) of the above three parameters, $C_Q(r_F)$. In other words, in the second procedure data were analyzed by non-linear least squares methods, using the equation:

$$A_t(r) = \frac{C_I(r_F)}{\varepsilon_I}\psi_I + \frac{\frac{C_I(r_F)}{\varepsilon_I}\cdot K_d}{\frac{C_{IQ}(r_F)}{\varepsilon_{IQ}}}\psi_I^{\,p} + \frac{C_{IQ}(r_F)}{\varepsilon_{IQ}}\psi_I^{\,p+1} \qquad \text{[Eq. 4]}$$

Figure 6 shows the results of these analyses. In the figure, the symbols are experimental data points, the thin black line is the analysis of the data using EQ. 3, and the somewhat thicker gray line represents the fit of the data using EQ. 4. As shown in the figure, the two fits are essentially superimposable. A mean value (± S.D.) of 0.74 ± 0.22 μM was obtained for K_d from the values of $C_I(r_F)$, $C_Q(r_F)$, and $C_{IQ}(r_F)$, which is in reasonable agreement with the values for K_d obtained from SPR of 0.92 μM.

The analysis also indicated that nearly all of the Q ($YAQ_{12}A$) remaining in solution is part of a complex. Although additional terms, corresponding to higher order complexes, could be added to the equation to fit the data, such terms did not improve the fit (Supporting Figure 3). Since the theoretical fits overlap completely and are indistinguishable from that obtained using the simpler equation, it is most parsimonious to conclude that the predominant complex is a 1:1 stoichiometric complex, also in agreement with SPR data. Finally, as discussed in Supporting Information, the fit of data to the model containing a complex was compared to that containing no complex, by using the Aikake Information Criterion (AIC, 21, 30). The AIC is a measure of the goodness of fit of an estimated statistical model that rewards goodness of fit (as determined by the sum of squares or χ^2), and also penalizes the number of parameters and therefore penalizes overfitting. Thus, in general, a lower AIC indicates a preferable model, i.e., the best fit of the data with a minimum number of free parameters. As indicated in Supporting Table 1, in all cases but one (which was a virtual tie) the inclusion of a term for a 1:1 complex, rather than only free I and free Q, lowered the AIC, indicating that this was a preferable model. In conclusion, the analytical ultracentrifugation data are consistent with a model in with $YAQ_{12}A$ forms mainly a 1:1 complex with $5QMe_2$.

Secondary Structure of $5QMe_2$ and Related Peptides

The CD spectrum of $YAQ_{12}A$ in solution shows a small maximum at ~ 220 nm, and a trough with a minimum at ~ 199 nm, consistent with a PPII-like helical structure (Figure 7A). When it forms fibrils, it undergoes a transition to β-sheet structure, as shown by film CD spectroscopy (Figure 7B), as do other short polyQ peptides (12, 31-34). The CD spectrum of $5QMe_2$ is also consistent with a left-handed, PPII-like structure (Figure 7A), though with a red-shifted maximum at ~ 232 nm, and a minimum at ~ 199 nm, possibly suggesting subtle structural differences from $YAQ_{12}A$. In contrast to $5QMe_2$, two of the less effective inhibitors, 5MeQ and $5MeQMe_2$ with backbone *N*-methylation, had CD spectra indicative of β-sheet (Figure 7C). These data suggest that the most effective inhibitor has a structure resembling the soluble form of its PPII target peptide, $YAQ_{12}A$, while the less

NIH-PA Author Manuscript

NIH-PA Author Manuscript

NIH-PA Author Manuscript

effective inhibitors have the structure, β-sheet, of the final fibrillar product of the aggregation pathway. A 1:1 mixture of $YAQ_{12}A$:$5QMe_2$ did not match an arithmetic weighted mean of the spectra of the two individual peptides (Figure 7A), which is consistent with above observations that the two peptides form a distinct complex.

Discussion

In this paper, we have described *N*-methylated inhibitors of polyQ peptide aggregation. $5QMe_2$, with only alternate side chain amides *N*-methylated, was far more effective than the others, including 5MeQ with only backbone *N*-methylations, and $5MeQMe_2$ with both backbone and side chain *N*-methylation. These results demonstrate the importance of side chain hydrogen bonding in polyglutamine fibrillation, which has been posited from molecular modeling (35,36). Also, the inhibitor in which alternate side chains were methylated ($5QMe_2$) was more effective than that in which all the side chains were methylated ($(QMe_2)_5$), indicating the need to retain some unmodified amides for binding to the aggregating target peptide.

Addition of $5QMe_2$ to $YAQ_{12}A$ at stoichiometric ratios or higher prevented disappearance of monomeric $YAQ_{12}A$ from solution for 40 h, although at 70 h, complete inhibition required higher stoichiometric ratios (e.g., $5QMe_2$:$YAQ_{12}A$ =10:1). These results suggest that $5QMe_2$ inhibits nucleation of $YAQ_{12}A$, but does not eliminate it. In addition, adding $5QMe_2$ to solutions of $YAQ_{12}A$ at various times after the start of fibrillation prevented all but a minor degree of further aggregation of $YAQ_{12}A$ for times up to 70h, suggesting that $5QMe_2$ also inhibits fibril elongation. Furthermore, $5QMe_2$ inhibited seeded fibrillation of $YAQ_{12}A$, which largely bypasses nucleation steps, suggesting that $5QMe_2$ is a fibril extension as well as a nucleation inhibitor. $5QMe_2$ causes $YAQ_{12}A$ to remain in a monomeric state rather than that of a soluble multimer. Thus, it is more properly called an aggregation inhibitor, rather than a fibrillation inhibitor.

SPR indicates very rapid binding and dissociation of a 1:1 complex, with moderate affinity (K_d = 0.92 μM). Both SPR and sedimentation equilibrium analytical ultracentrifugation suggest that the predominant complex formed by $5QMe_2$ and $YAQ_{12}A$ has a 1:1 stoichiometry. The rapidity with which the complex dissociated was also shown by size exclusion chromatography, where both $5QMe_2$ and $YAQ_{12}A$ eluted at a position most consistent with monomeric MW^{app}. Chromatography of a mixture of these peptides yielded two peaks, in the same elution positions as the individual peptide, indicating complete dissociation of complex during the chromatography. (For further discussion of this point, see Supporting Information and Supporting Figures 4A and B.) This binding pattern of target peptides is reminiscent of chaperone proteins, which also bind their targets with moderate affinity, but have very high k_{on} and k_{off}. Rates have been measured for Hsp70 and Hsp90 (37, 38) (though these particular chaperonins do not bind polyQ peptides). Although it is sometimes assumed that a high affinity indicates a better aggregation inhibitor, this is not necessarily the case. $5QMe_2$ is notable for acting at sub-stoichiometric levels, suggesting that the kinetics of complex association and dissociation are faster than the kinetics of $YAQ_{12}A$ aggregation. Thus, the effectiveness of $5QMe_2$ is likely due to fast k_{on} *and* k_{off} rates, and could be hampered by a higher affinity.

Thus, $5QMe_2$, like chaperones, may keep aggregation-prone peptides or proteins in a less aggregation-prone conformation, e.g., by preventing β-sheet formation. Indeed, CD spectroscopy shows that $5QMe_2$ does *not* have a β-strand structure. Rather, its spectrum is most consistent with a PPII helical conformation. In contrast, the backbone modified peptides, 5MeQ and $5MeQMe_2$, showed β-strand structure by CD (Figure 7C), and were less effective inhibitors than $5QMe_2$. It is striking that the secondary structure of $5QMe_2$

NIH-PA Author Manuscript

NIH-PA Author Manuscript

NIH-PA Author Manuscript

resembles that of its target peptide, a property that may be generalizable to all *N*-methylated inhibitors. Indeed, when we added $5QMe_2$ to $YAQ_{12}A$, both reactants had structures consistent with PPII or PPII-like helices by CD spectroscopy (although not identical CD spectra), and the products in the mixture also had a PPII structure. Similarly, inhibitors of Aβ aggregation, such as the backbone *N*-methylated peptide, Aβ16-20m (16, 17) have similar secondary structure as their targets, but in those cases, β-sheet.

These results are consonant with our recent observations (18) that short peptides containing a QQQ triplet, aggregate into soluble oligomeric species *as PPII helices*, although they are too short ever to form fibrils or adopt a β-sheet structure. Longer polyQ peptides, such as $YAQ_{12}A$, can form insoluble β-sheets, but as soluble monomers, have a PPII helical structure. The PPII conformation is also stabilized in polyQ segments by a polyproline segments adjacent to the C-terminal end of the polyQ segment (12,39).

The foregoing also helps to explain the fact that, in contrast to Aβ16-20m and other backbone-modified aggregation inhibitors of β-amyloid and prion peptide aggregation (16,17,40,41), $5QMe_2$ did not disassemble pre-formed fibrils. $5QMe_2$ interacts with soluble (PPII-like) $YAQ_{12}A$, but apparently not with fibrillar (β-sheet) $YAQ_{12}A$. $5QMe_2$ also prevents fibril elongation, possibly by interacting with $YAQ_{12}A$ still in solution. A model of $5QMe_2$ action is depicted in Figure 8. According to this model, $YAQ_{12}A$ exists in solution as PPII-like monomer. It is possible that this peptide can also forming oligomers, but we did not observe this, suggesting that oligomers, if present, were at very low concentrations or were short-lived. Progression to fibril formation requires a transition from PPII to β-sheet conformation, of $YAQ_{12}A$ monomers, oligomers, or both. $5QMe_2$ forms transient 1:1 complexes with $YAQ_{12}A$ monomers, thereby maintaining the latter peptide in a PPII-like state. Binding of $5QMe_2$ appears to inhibit formation of hydrogen bonds between side chains of $YAQ_{12}A$ molecules. The fact that $5QMe_2$ both maintains $YAQ_{12}A$ in a monomeric PPII-like state, and also prevents this peptide from forming fibrils suggests that some species with PPII structure may be on-pathway for fibril formation.

Finally, it is appropriate to address the relevance of $YAQ_{12}A$ to aggregation of longer polyQ proteins in biological contexts. PolyQ peptides and proteins have a sharp threshold for aggregation into fibrils, but this threshold is context dependent (12,42,43). In the context of the protein huntingtin, this threshold is ~ 35 glutamine residues, as is shown by the occurrence of disease in people with CAG triplet expansions of the gene (1), in model systems such as *C. elegans* and *S. cerevisiae* (44,45), and in studies of recombinant htt exon 1-encoded protein *in vitro* (2,3). In spinocerebellar ataxia (SCA) type 6 however, the threshold for disease is considerably shorter. The gene for this disease encodes the $\alpha 1_A$-voltage-dependent calcium channel subunit, and disease and intracellular protein aggregates occur when the polyQ expansion exceeds 20-30 residues (46). For peptides without neighboring domains, even as few as six Q residues is sufficient to form β-sheet-rich fibrils (12), and $YAQ_{12}A$ clearly is above this threshold (Figure 7B). Thus, while the threshold might change with context, inhibitors such as $5QMe_2$ can serve as structural probes of the aggregation pathway of biologically relevant polyQ peptides and proteins. Finally, although we have used this inhibitor peptide primarily as a structural probe, it could possibly also serve as the basis of an avenue of therapeutic approach.

Supplementary Material

Refer to Web version on PubMed Central for supplementary material.

NIH-PA Author Manuscript

NIH-PA Author Manuscript

NIH-PA Author Manuscript

Acknowledgments

We thank Hélène Auer for assistance with peptide synthesis and purification, and Gregory Darnell for helpful discussions. We thank Yimei Chen of the Electron Microscopy Facility, Elena Solomaha of the Biophysics Facility, and Jin Qin at the Chemistry Mass Spectrometry Facility, at the University of Chicago.

Abbreviations

AIC	Aikake Information Criterion
Anth	*N*-methyl anthranilic acid
BOP	benzotriazole-1-yl-oxy-tris-(dimethylamino)-phosphonium hexafluorophosphate
CD	Circular dichroic
DMF	dimethylformamide
ESI	electrospray ionization
FMOC	9-fluorenylmethoxycarbonyl
Glu(tBu)	N-α-FMOC-L-glutamic acid γ-*tert*-butyl ester
HATU	2-(7-Aza-1H-benzotriazole-1-yl)-1,1,3,3-tetramethyluronium hexafluorophosphate
HD	Huntington's Disease
HPLC	high performance liquid chromatography
MALDI-TOF	matrix assisted laser desorption-time of flight
MBHA	4-Methylbenzhydrylamine
PEG	polyethyleneglycol
polyP	polyproline
polyQ	polyglutamine
PPII	polyproline type II
S.D.	standard deviation
SPR	surface plasmon resonance
TFA	trifluoroacetic acid

References

1. The Huntington's Disease Collaborative Research Group. A novel gene containing a trinucleotide repeat that is expanded and unstable on Huntington's disease chromosomes. Cell. 1993; 72:971–983. [PubMed: 8458085]
2. Scherzinger E, Lurz R, Turmaine M, Mangiarini L, Hollenbach B, Hasenbank R, Bates GP, Davies SW, Lehrach H, Wanker EE. Huntingtin-encoded polyglutamine expansions form amyloid-like protein aggregates *in vitro* and *in vivo*. Cell. 1997; 90:549–558. [PubMed: 9267034]
3. Scherzinger E, Sittler A, Schweiger K, Heiser V, Lurz R, Hasenbank R, Bates GP, Lehrach H, Wanker EE. Self-assembly of polyglutamine-containing huntingtin fragments into amyloid-like fibrils: implications for Huntington's disease pathology. Proc. Natl. Acad. Sci. USA. 1999; 96:4604–4609. [PubMed: 10200309]
4. Davies SW, Turmaine M, Cozens BA, DiFiglia M, Sharp AH, Ross CA, Scherzinger E, Wanker EE, Mangiarini L, Bates GP. Formation of neuronal intranuclear inclusions underlies the neurological dysfunction in mice transgenic for the HD mutation. Cell. 1997; 90:537–548. [PubMed: 9267033]

NIH-PA Author Manuscript

NIH-PA Author Manuscript

NIH-PA Author Manuscript

5. Chen S, Berthelier V, Hamilton JB, O'Nuallain B, Wetzel R. Amyloid-like features of polyglutamine aggregates and their assembly kinetics. Biochemistry. 2002; 41:7391–7399. [PubMed: 12044172]
6. Sharma D, Shinchuk LM, Inouye H, Wetzel R, Kirschner DA. Polyglutamine homopolymers having 8–45 residues form slablike β-crystallite assemblies. Proteins: Struct., Funct., Bioinf. 2005; 61:398–411.
7. Petkova AT, Ishii Y, Balbach JJ, Antzutkin ON, Leapman RD, Delaglio F, Tycko R. A structural model for Alzheimer's β-amyloid fibrils based on experimental constraints from solid state NMR. Proc. Natl. Acad. Sci. USA. 2002; 99:16742–16747. [PubMed: 12481027]
8. Shewmaker F, Wickner RB, Tycko R. Amyloid of the prion domain of Sup35p has an in-register parallel β-sheet structure. Proc. Natl. Acad. Sci. USA. 2006; 103:19754–19759. [PubMed: 17170131]
9. Wickner RB, Dyda F, Tycko R. Amyloid of Rnq1p, the basis of the [PIN^+] prion, has a parallel in-register β-sheet structure. Proc. Natl. Acad. Sci. USA. 2008; 105:2403–2408. [PubMed: 18268327]
10. Chimon S, Ishii Y. Capturing intermediate structures of Alzheimer's β-amyloid, Aβ(1-40), by solid-state NMR spectroscopy. J. Am. Chem. Soc. 2005; 127:13472–13473. [PubMed: 16190691]
11. Poirier MA, Li H, Macosko J, Cai S, Amzel M, Ross CA. Huntingtin spheroids and protofibrils as precursors in polyglutamine fibrilization. J. Biol. Chem. 2002; 277:41032–41037. [PubMed: 12171927]
12. Darnell G, Orgel JPRO, Pahl R, Meredith SC. Flanking polyproline sequences inhibit β-sheet structure in polyglutamine segments by inducing PPII-like helix structure. J. Mol. Biol. 2007; 374:688–704. [PubMed: 17945257]
13. Nagai Y, Tucker T, Ren H, Kenan DJ, Henderson BS, Keene JD, Strittmatter WJ, Burke JR. Inhibition of polyglutamine protein aggregation and cell death by novel peptides identified by phase display screening. J. Biol. Chem. 2000; 275:10437–10442. [PubMed: 10744733]
14. Nagai Y, Fujikake N, Ohno K, Higashiyama H, Popiel HA, Rahadian J, Yamaguchi M, Strittmatter WJ, Burke JR, Toda T. Prevention of polyglutamine oligomerization and neurodegeneration by the peptide inhibitor QBP1 in Drosophila. Hum. Mol. Genet. 2003; 12:1253–1260. [PubMed: 12761040]
15. Thakur AK, Yang W, Wetzel R. Inhibition of polyglutamine aggregate cytotoxicity by a structure-based elongation inhibitor. FASEB J. 2004; 18:923–925. [PubMed: 15001566]
16. Gordon DJ, Sciarretta KL, Meredith SC. Inhibition of β-amyloid(40) fibrillogenesis and disassembly of β-amyloid(40) fibrils by short beta-amyloid congeners containing N-methyl amino acids at alternate residues. Biochemistry. 2001; 40:8237–8245. [PubMed: 11444969]
17. Gordon DJ, Tappe R, Meredith SC. Design and characterization of a membrane permeable N-methyl amino acid-containing peptide that inhibits Aβ1-40 fibrillogenesis. J. Pept. Res. 2002; 60:37–55. [PubMed: 12081625]
18. Darnell GD, Derryberry JM, Kurutz JW, Meredith SC. Mechanism of Cis-Inhibition of PolyQ Fibrillation by PolyP: PPII Oligomers and the Hydrophobic Effect. Biophys. J. 2009; 97:2295–2305. [PubMed: 19843462]
19. Biron E, Chatterjee J, Kessler H. Optimized selective *N*-methylation of peptides on solid support. J. Pept. Sci. 2006; 12:213–219. [PubMed: 16189816]
20. O'Nuallain B, Thakur AK, Williams AD, Bhattacharyya AM, Chen S, Thiagarajan G, Wetzel R. Kinetics and thermodynamics of amyloid assembly using a high-performance liquid chromatography-based sedimentation assay. Methods Enzymol. 2006; 413:34–74. [PubMed: 17046390]
21. Yamaoka K, Tanigawara Y, Nakagawa T, Uno T. A pharmacokinetic analysis program (MULTI) for microcomputer. J. Pharm. Dyn. 1981; 4:879–885.
22. De Mol, NJ.; Fischer, MJE. Kinetic and Thermodynamic Analysis of Ligand–Receptor Interactions: SPR Applications in Drug Development. In: Schasfoort, RBM.; Tudos, AJ., editors. Handbook of Surface Plasmon Resonance. First edition. RSC Publishing; London, U.K.: 2008. p. 123-172.

NIH-PA Author Manuscript

NIH-PA Author Manuscript

NIH-PA Author Manuscript

23. Winzor DJ, Jacobsen MP, Wills PR. Direct Analysis of Sedimentation Equilibrium Distributions Reflecting Complex Formation between Dissimilar Reactants. Biochemistry. 1998; 37:2226–2233. [PubMed: 9485368]
24. Milthorpe BK, Jeffrey PD, Nichol LW. The direct analysis of sedimentation equilibrium results obtained with polymerizing systems. Biophys. Chem. 1975; 3:169–176. [PubMed: 1148373]
25. Nichol LW, Jeffrey PD, Milthorpe BK. The sedimentation equilibrium of heterogeneously associating systems and mixtures of non-interacting solutes: analysis without determination of molecular weight averages. Biophys. Chem. 1976; 4:259–267. [PubMed: 949527]
26. Jeffrey PD, Nichol LW, Teasdale RD. Studies of macromolecular heterogeneous associations involving cross-linking: a re-examination of the ovalbumin-lysozyme system. Biophys. Chem. 1979; 10:379–387. [PubMed: 534683]
27. Lebowitz J, Lewis MS, Schuck P. Modern analytical ultracentrifugation in protein science: A tutorial review. Protein Sci. 2002; 11:2067–2079. [PubMed: 12192063]
28. Pallitto MM, Murphy RM. A mathematical model of the kinetics of beta-amyloid fibril growth from the denatured state. Biophys. J. 2001; 81:1805–1822. [PubMed: 11509390]
29. Bhattacharyya AM, Thakur AK, Wetzel R. Polyglutamine aggregation nucleation: Thermodynamics of a highly unfavorable protein folding reaction. Proc. Natl. Acad. Sci. USA. 2005; 102:15400–15405. [PubMed: 16230628]
30. Akaike H. A new look at the statistical model identification". IEEE Transactions on Automatic Control. 1974; 19:716–723.
31. Chellgren BW, Miller AF, Creamer TP. Evidence for polyproline II helical structure in short polyglutamine tracts. J. Mol. Biol. 2006; 361:362–371. [PubMed: 16854433]
32. Shi Z, Chen K, Liu Z, Sosnick TR, Kallenbach NR. PPII structure in the model peptides for unfolded proteins: studies on ubiquitin fragments and several alanine-rich peptides containing QQQ, SSS, FFF, and VVV. Proteins: Struct., Funct., Bioinf. 2006; 63:312–321.
33. Chellgren BW, Creamer TP. Short sequences of non-proline residues can adopt the polyproline II helical conformation. Biochemistry. 2004; 43:5864–5869. [PubMed: 15134460]
34. Shi Z, Woody RW, Kallenbach NR. Is polyproline II a major backbone conformation in unfolded proteins? Adv. Prot. Chem. 2002; 62:163–240.
35. Starikov EB, Lehrach H, Wanker EE. Folding of oligoglutamines: a theoretical approach based on thermodynamics and molecular mechanics. J. Biomol. Struct. Dyn. 1999; 17:409–427. [PubMed: 10636078]
36. Esposito L, Paladino A, Pedone C, Vitagliano L. Insights into structure, stability, and toxicity of monomeric and aggregated polyglutamine models from molecular dynamics simulations. Biophys. J. 2008; 94:4031–4040. [PubMed: 18234827]
37. Miyata Y, Yahara I. Interaction between Casein Kinase II and the 90-kDa stress protein, HSP90. Biochemistry. 1995; 34:8123–8129. [PubMed: 7794926]
38. Maeda H, Sahara H, Mori Y, Torigo T, Kamiguchi K, Tamura Y, Tamura Y, Hirata K, Sato N. Biological heterogeneity of the peptide-binding motif of the 70-kDa heat shock protein by surface plasmon resonance analysis. J. Biol. Chem. 2007; 282:26956–26962. [PubMed: 17626008]
39. Bhattacharyya A, Thakur AK, Chellgren VM, Thiagarajan G, Williams AD, Chellgren BW, Creamer TP, Wetzel R. Oligoproline effects on polyglutamine conformation and aggregation. J. Mol. Biol. 2006; 355:524–535. [PubMed: 16321399]
40. Madine J, Doig AJ, Middleton DA. Design of an N-Methylated Peptide Inhibitor of α-Synuclein Aggregation Guided by Solid-State NMR. J. Am. Chem. Soc. 2008; 130:7831–7881.
41. Hughes E, Burke RM, Doig AJ. Inhibition of toxicity in the β-amyloid peptide fragment β-(25-35) using N-methylated derivatives: a general strategy to prevent amyloid formation. J. Biol. Chem. 2000; 275:25109–25115. [PubMed: 10825171]
42. Nozaki K, Onodera O, Takano H, Tsuji S. Amino acids flanking polyglutamine stretches influence their potential for aggregate formation. NeuroReport. 2001; 12:3357–3364. [PubMed: 11711886]
43. Shizuka M, Watanabe M, Ikeda Y, Mizushima K, Okamoto K, Shoji M. Molecular analysis of a de novo mutation for spinocerebellar ataxia type 6 and (CAG)n repeat units in normal elder controls. J. Neurol. Sci. 1998; 161:85–87. [PubMed: 9879686]

NIH-PA Author Manuscript

NIH-PA Author Manuscript

NIH-PA Author Manuscript

44. Morley JF, Brignull HR, Weyers JJ, Morimoto RI. The threshold for polyglutamine-expansion protein aggregation and cellular toxicity is dynamic and influenced by aging in *Caenorhabditis elegans*. Proc. Natl. Acad. Sci. USA. 2002; 99:10417–10422. [PubMed: 12122205]

45. Krobitsch S, Lindquist S. Aggregation of huntingtin in yeast varies with the length of the polyglutamine expansion and the expression of chaperone proteins. Proc. Natl. Acad. Sci. USA. 2000; 97:1589–1594. [PubMed: 10677504]

46. Shizuka M, Watanabe M, Ikeda Y, Mizushima K, Okamoto K, Shoji M. Molecular analysis of a de novo mutation for spinocerebellar ataxia type 6 and (CAG)n repeat units in normal elder controls. J. Neurol. Sci. 1998; 161:85–87. [PubMed: 9879686]

NIH-PA Author Manuscript

NIH-PA Author Manuscript

NIH-PA Author Manuscript

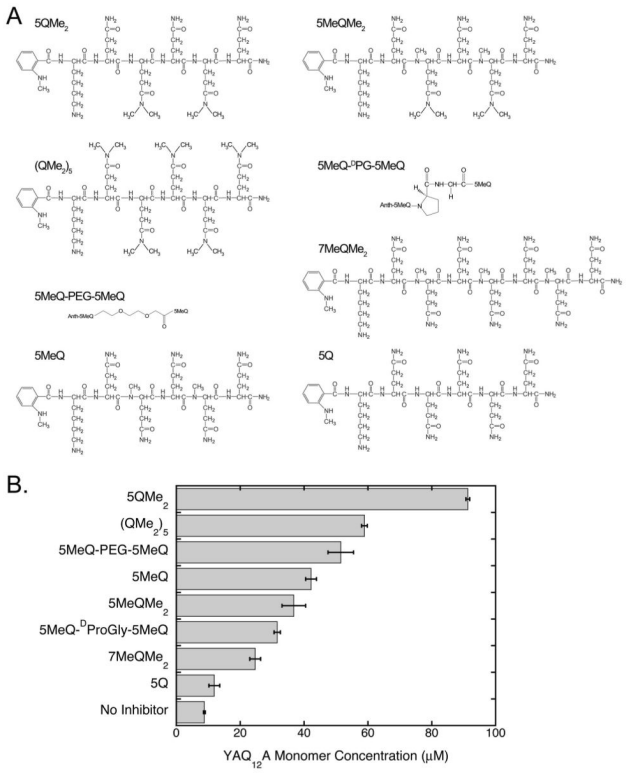

Figure 1.

Structures of inhibitors tested (A), and results of sedimentation screening assays (B). The peptides represent variations in the pattern of *N*-methylation. In all cases, the peptides contained an N-terminal *N*-methylanthranilic acid (Anth) and a Lys residue adjacent to the Anth. In the case of 5MeQ-^{D}PG-5MeQ and 5MeQ-PEG-5MeQ, the C-terminal inhibitor domain does not contain a Lys residue. Results are expressed as concentration of μM $YAQ_{12}A$ monomer remaining after the incubation. Data are the mean ± S.D. of three replicate determinations.

NIH-PA Author Manuscript

NIH-PA Author Manuscript

NIH-PA Author Manuscript

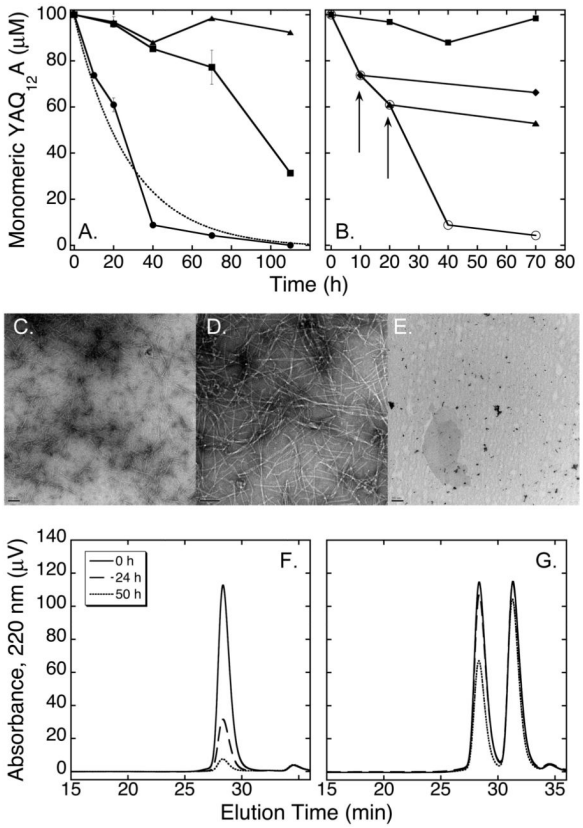

Figure 2.

Time course of $YAQ_{12}A$ aggregation and inhibition by $5QMe_2$; electron microscopy of reaction products; size exclusion chromatography of $YAQ_{12}A$ in the absence or presence of $5QMe_2$. (A) Aggregation of 100 μM $YAQ_{12}A$ in the absence of $5QMe_2$ (λ), or the presence of 100 μM (ν) or 1.0 mM (σ) $5QMe_2$ (mean ± S.D. of three replicates); the dotted line represents a least squares fit to a mono-exponential equation. $YAQ_{12}A$ remaining in solution at various time points in the incubation was measured using the sedimentation assay described in Methods and originally described in (20). (B) Effect of adding $5QMe_2$ to $YAQ_{12}A$ at different points in the aggregation time course. 1 mM $5QMe_2$ was added to 100 μM $YAQ_{12}A$ at t = 0 h (ν), or after $YAQ_{12}A$ had been allow to aggregate for 10h (ν) or 20 h (σ); (○) is no inhibitor. Results are monomeric $YAQ_{12}A$ remaining in solution at various time points. (C), (D), and (E) Electron micrographs of 100 μM $YAQ_{12}A$ incubated for 40 h at 37 °C in the absence (C and D) or presence (E) of 500 μM $5QMe_2$. No grossly visible precipitate was present for $YAQ_{12}A$ incubated in the presence of inhibitor. The figures show 15,000 × magnification (C and E) or 49,000 × magnification (D), with scale bars of 100 (C and E) or 200 nm (D), respectively. (F) and (G) Size exclusion chromatography of 100 μM disaggregated $YAQ_{12}A$ alone (F) or in the presence of 170 μM $5QMe_2$ (G). 100 μL aliquots of these solutions were chromatographed at 0, 24 and 50 h (black, blue, and red, respectively). Chromatography was performed using a Superdex Peptide 10/300 column; effluent was 10 mM sodium phosphate containing 10 mM NaCl, pH 7.40, and flow rate was 0.5 mL/min. Column effluent was monitored at 220, 230, 274 and 337 nm; the chromatograph shown was monitored at 230 nm. $YAQ_{12}A$ elutes as a single peak with an elution time most consistent with MW^{app} ~ 1805.5, close to the actual molecular weight of 1860. $5QMe_2$ elutes somewhat later, at a position consistent with monomer (MW^{app} ~ 1176.0).

NIH-PA Author Manuscript

NIH-PA Author Manuscript

NIH-PA Author Manuscript

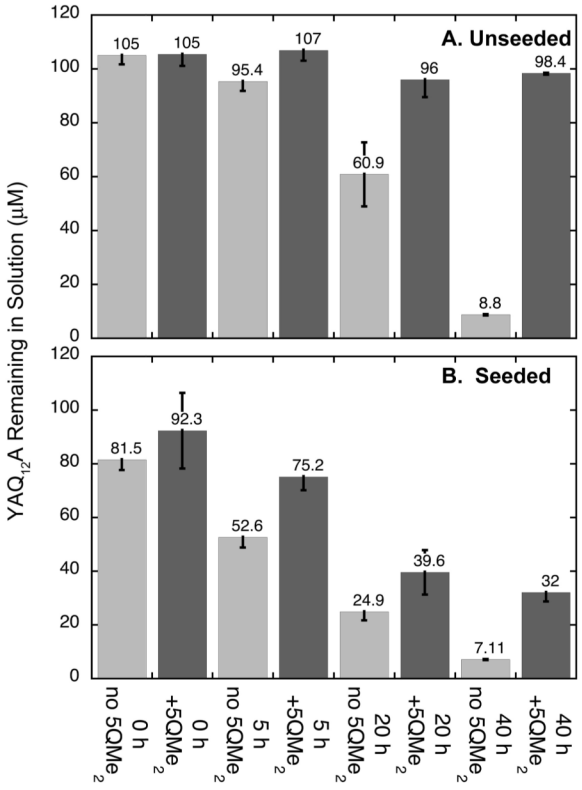

Figure 3.

Effect of $5QMe_2$ on seeded and unseeded fibrillation of $YAQ_{12}A$. (A) A freshly disaggregated, 100 μM solution of $YAQ_{12}A$ was incubated in the presence or absence of 100 μM $5QMe_2$, as described in Methods, and then was assayed for $YAQ_{12}A$ remaining in solution at 0, 5, 20 and 40 h. (B) A freshly disaggregated, 100 μM solution of $YAQ_{12}A$ was incubated with an pre-formed $YAQ_{12}A$ fibril seeds at a nominal concentration of 8 μM (i.e., seed $YAQ_{12}A$: soluble $YAQ_{12}A$ = 100:8, mol:mol), in the presence or absence of 100 μM $5QMe_2$, as described in Methods, and $YAQ_{12}A$ remaining in solution was assayed as in Panel (A). Results are means (± S.D.) of three determinations, reported in μM $YAQ_{12}A$ remaining in solution.

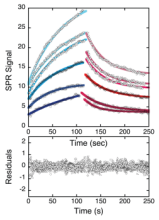

Figure 4.

Surface plasmon resonance of immobilized $YAQ_{12}A$ interacting with soluble $5QMe_2$. (A) SPR data showing binding and subsequent dissociation of $5QMe_2$ at various concentrations, ranging from 5 to 50 μM, to and from immobilized $YAQ_{12}A$. In the figure, points represent experimental data, and solid lines are non-linear least squares fits of the data to monoexponential kinetics of binding and desorption. (B) Residuals were calculated as the difference between experimental data and calculated values using the parameters obtained from non-linear least squares fits. For both panels, concentrations of $5QMe_2$ were: (○), 5 μM; (□), 10 μM; (◇), 20 μM; (△), 30 μM; (▽), 40 μM; (▷), 50 μM.

NIH-PA Author Manuscript NIH-PA Author Manuscript NIH-PA Author Manuscript

NIH-PA Author Manuscript

NIH-PA Author Manuscript

NIH-PA Author Manuscript

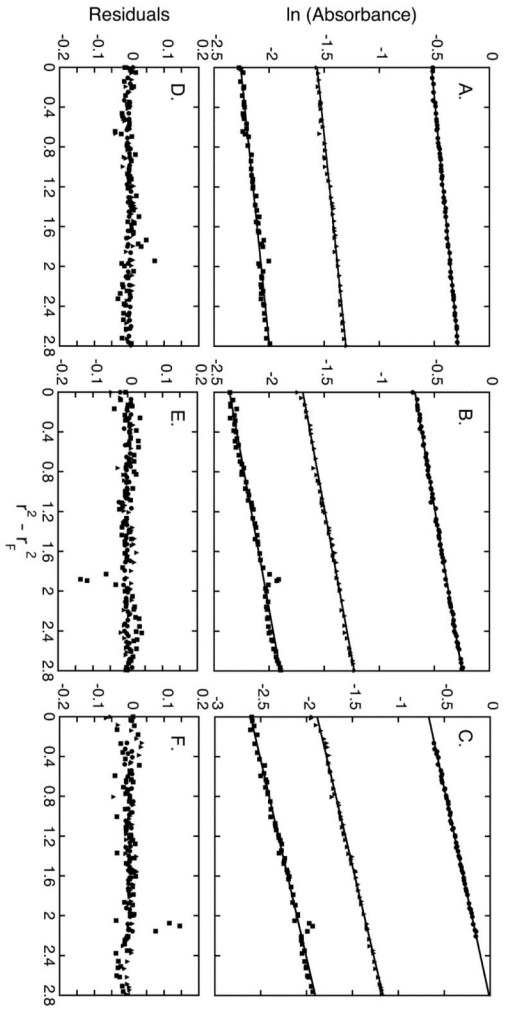

Figure 5.

Sedimentation of $5QMe_2$ alone, at 100 (ν), 500 (σ), and 1000 (λ) μM, and at 36,000 (A), 48,000 (B), and 60,000 (C) rpm. Conditions were as described in Experimental Procedures.

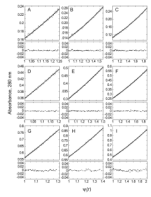

Figure 6.

Sedimentation equilibrium analytical ultracentrifugation of $YAQ_{12}A$ and $5QMe_2$ mixtures. The figure shows a mixtures of 100 μM $YAQ_{12}A$ and 100 (A, B, C), 500 (D, E, F) or 1000 (G, H, I) μM $5QMe_2$ centrifuged to equilibrium at 36,000 (A, D, G), 48,000 (B, E, H) or 60,000 (C, F, I) rpm. Concentrations were monitored by absorbance at 230 nm (A, B, C) or 280 nm (D-I) to obtain the desired level of sensitivity. The symbols are experimental data points, the thin black line is the analysis of the data using EQ. 3, and the thicker gray line represents the fit of the data using EQ. 4. For all panels, the bottom graph shows residual values, calculated as the difference between experimental and theoretical values calculated from the parameters obtained from non-linear least squares fit.

NIH-PA Author Manuscript NIH-PA Author Manuscript NIH-PA Author Manuscript

NIH-PA Author Manuscript
NIH-PA Author Manuscript
NIH-PA Author Manuscript

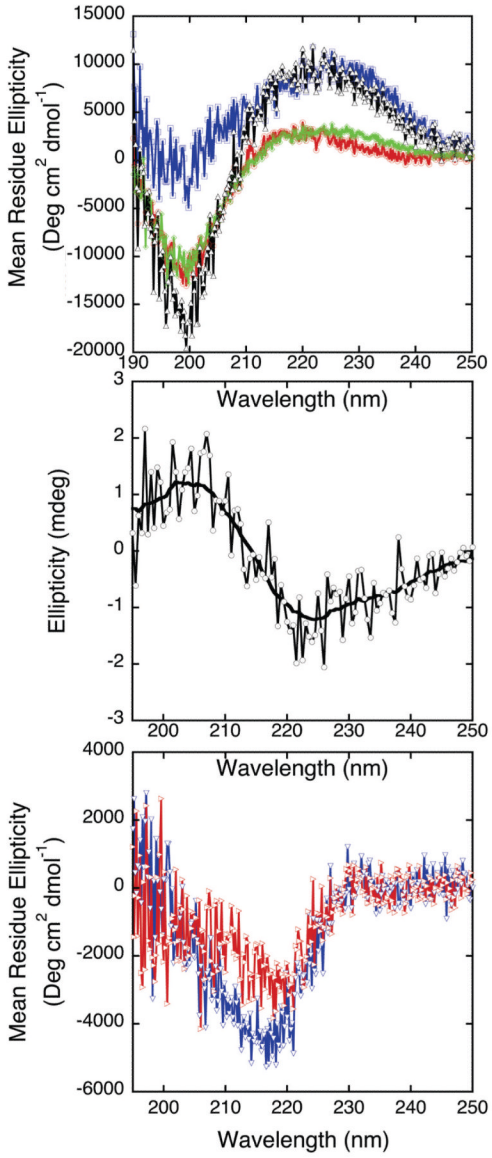

Figure 7.

(A) CD spectroscopy of $YAQ_{12}A$, $5QMe_2$, and an equimolar mixture of the two peptides. Circular dichroic spectra of $YAQ_{12}A$ (100 μM, ○), $5QMe_2$ (100 μM, □), and an equimolar mixture of the two peptides (100 μM of each peptide, ◇). Also shown is a calculated weighted mean of the two spectra of $YAQ_{12}A$ and $5QMe_2$ alone (△). Points are experimental data; lines represented curves smoothed using the smooth macro of Kaleidagraph software. For clarity, only every third point is shown in the figure. (B) Circular dichroic spectrum of $YAQ_{12}A$ fibril films. The procedure was essentially as described by Darnell *et al*. (12). (C) CD spectra of 5MeQ (▽) and $5MeQMe_2$ (▷) under the same conditions as described for Panel A.

NIH-PA Author Manuscript
NIH-PA Author Manuscript
NIH-PA Author Manuscript

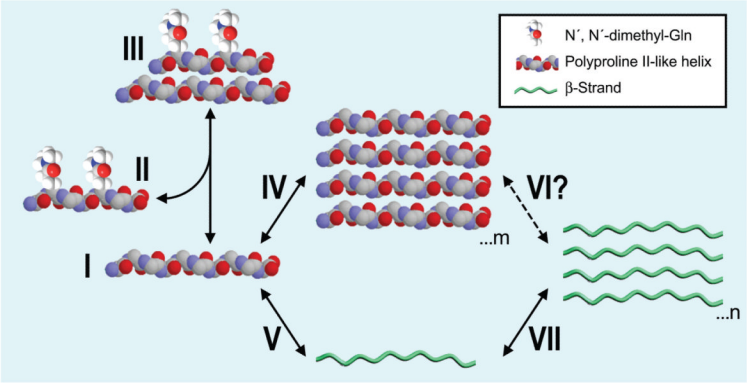

Figure 8.

Schema depicting model of inhibition of polyQ aggregation by $5QMe_2$. $YAQ_{12}A$ has PPII-like structure in solution (**I**), as do other polyQ peptides (12,31-34). $5QMe_2$ (**II**) also has a PPII-like conformation, and is predominantly or entirely monomeric in solution. $5QMe_2$ rapidly binds $YAQ_{12}A$ and forms transient complexes (**III**). PolyQ peptides have been shown to form oligomers with a PPII-like conformation (**IV**,18), and it is not known whether these are on- or off-pathway for fibril formation (**VI**). Monomeric $YAQ_{12}A$ could also undergo a PPII to β-strand transition (**V**), as has been proposed for other polyQ peptides (31-34), and these could self-associate into fibrils (**VII**). The inhibitor is chaperone-like in it binds and releases its target very rapidly, presumably more rapid than nucleation of $YAQ_{12}A$ itself. The side chain *N*-methyl groups of $5QMe_2$ result in the formation of predominantly 1:1 stoichiometric complexes with $YAQ_{12}A$, blocking oligomerization of the peptides in this complex, and delaying the transition from PPII to β-strand or β-sheet.

NIH-PA Author Manuscript

NIH-PA Author Manuscript

NIH-PA Author Manuscript

Table 1

Inhibition of $YAQ_{12}A$ by $5QMe_2$ at various concentration ratios

$5QMe_2$ (mM)	Concentration Ratio of $5QMe_2$: $YAQ_{12}A$ (mol:mol)*	$YAQ_{12}A$ Monomer Remaining
4.00	40	91.3 ± 0.6
1.00	10	87.9 ± 0.3
0.50	5	95.2 ± 0.4
0.10	1	85.2 ± 0.4
0.05	0.5	90.1 ± 1.5
0.025	0.25	42.0 ± 0.8
0.01	0.1	36.3 ± 11.4

* In all cases, $YAQ_{12}A$ was at 100 μM at the start of the reaction. Incubation was for 40 h at 37 °C. Monomeric $YAQ_{12}A$ remaining in solution after the incubation was measured by RP-HPLC, as described in Methods.